

Intraseasonal Variability of Hail in the Contiguous United States: Relationship to the Madden–Julian Oscillation

BRADFORD S. BARRETT AND BRITTANY N. HENLEY

Oceanography Department, U.S. Naval Academy, Annapolis, Maryland

(Manuscript received 3 August 2014, in final form 9 December 2014)

ABSTRACT

Climatologies have been developed to highlight variability of the frequency and intensity of hail in the United States. However, the intraseasonal variability of hail, including why one week might be active while the following inactive despite both having similar climatological probabilities, has not yet been explored. This paper presents relationships between spring-season (April–June) hail days and the leading mode of atmospheric intraseasonal variability, the Madden–Julian oscillation (MJO). It extends recent work on intraseasonal tornado variability to smaller spatial scales. In April, May, and June, statistically significant variability in hail days was found for different Real-time Multivariate MJO (RMM) phases of the MJO. For April, the strongest correlations between hail-day anomalies and anomalies of the product of convective available potential energy (CAPE) and 0–6-km vertical wind shear were found in RMM phase 5, with above-normal likelihood of a hail day found in the south-central United States. For May, the strongest correlations were found in RMM phase 3, with below-normal likelihood of a hail day located over the north-central United States. For June, the strongest correlations were found in phase 8, with above-normal likelihood of hail in west Texas and below-normal likelihood of hail over much of the middle of the United States. In all phases, 300-hPa height anomalies in the United States formed part of a global wave train similar to MJO patterns in both modeling and observational studies.

1. Introduction

Damaging hail occurs in the United States, on average, 158 days yr⁻¹ (Changnon et al. 2009). Including property and crop losses, annual U.S. hail damage routinely exceeds \$1 billion (U.S. dollars) (Changnon 1999; Changnon and Changnon 2009). Given this significant economic impact, scientific research on hail, including studies on formation, microphysics, prediction, remote detection, occurrence, and growth has been ongoing for decades (e.g., Douglas 1963; Browning 1977; Knight and Knight 2001). Furthermore, climatologies of hail have been developed to show how often hail occurs at a particular location and also its intensity (size) when it occurs (e.g., Changnon 2002; Schaefer et al. 2004; Doswell et al. 2005; Cecil and Blankenship 2012; Cintineo et al. 2012; Allen et al. 2015). These climatologies provide an important record of both past events and historical trends that is useful to insurance, agriculture, and operational

and research meteorology sectors. Hail climatologies are often smoothed in space and time to highlight the spatio-temporal progression of regions with enhanced hail frequency over their annual cycle. For example, the gridded hail climatology product currently operationally maintained by the NOAA Storm Prediction Center (SPC) first smooths hail probability in time using a 15-day Gaussian filter and then in space using a two-dimensional 120-km Gaussian filter (see <http://www.spc.noaa.gov/new/SVRclimo/climo.php?parm=allHail> for more details). The resulting climatology product, one of many similar such climatologies that have been developed, shows the seasonal variability of the likelihood of hail within 25 n mi (1 n mi = 1.852 km) of any point in the United States. It highlights the seasonality of daily hail probabilities, which peak in mid-May at approximately a 5% chance of hail within 25 n mi of a point. The climatological maximum shifts during the year, starting in the lower Mississippi valley in January, moving northward and westward to the central and northern high plains in July, and then moving back to the southeast in the autumn months.

The SPC and other similar climatologies particularly show the seasonal variability of hail occurrence, as discussed above. However, what is not evident are reasons

Corresponding author address: Bradford S. Barrett, Oceanography Department, U.S. Naval Academy, 572C Holloway Rd., Annapolis, MD 21402.
E-mail: bbarrett@usna.edu

for variability of hail occurrence within a season, the *intraseasonal* variability, which might explain why one week may be particularly active and the following week particularly inactive, despite both having similar hail probabilities on the seasonal time scale. Thus, the primary objective of this present study is to examine the variability of spring-season (April–June) hail by phase of the leading mode of atmospheric intraseasonal variability, the Madden–Julian oscillation [MJO; [Madden and Julian \(1972\)](#); phase defined by [Wheeler and Hendon \(2004\)](#)]. This study builds on other recent studies that found statistically significant relationships between spring-season tornadoes and the MJO ([Thompson and Roundy 2013](#), hereafter **TR13**; [Barrett and Gensini 2013](#), hereafter **BG13**). Tornadoes and hail often occupy a similar environmental phase space, suggesting that the relationship between the MJO and tornadoes may also be present for hail ([Brooks 2013](#)). This current study extends the MJO-tornado studies by exploring hail variability on a smaller scale. Both **TR13** and **BG13** considered variability in tornado activity for large regions of the country, but in this study, hail variability was examined on a 2° by 2° grid. By examining hail on this smaller scale, important details, such as dipolelike variability patterns, are visible that would be missed by considering the United States (or large regions of the United States) as a whole. Here, we focused on April–June instead of March–May because hail probabilities in June are higher than March.

The microphysical and kinematic processes for hail formation are complex ([Foote and Knight 1977](#); [Browning 1977](#); [Hughes and Wood 1993](#); [Brandes et al. 1997](#); [Emersic et al. 2011](#); [Ryzhkov et al. 2013](#)). However, the environmental characteristics favorable for hail formation are generally known: high instability [which can be quantified on the parcel scale by convective available potential energy (CAPE)], low environmental wet-bulb zero (WBZ) level, steep midlevel lapse rates, low environmental relative humidity, and high vertical wind shear ([Knight and Knight 2001](#)). Both vertical wind shear, which interacts with the updraft creating vertical perturbation pressure gradients ([Weisman and Klemp 1984](#); [Brooks and Wilhelmson 1990](#); [McCaull 1990](#)), and instability contribute to vertical accelerations necessary to support the growth of hail to severe size [currently defined by the National Weather Service to be a diameter ≥ 2.54 cm; [Ferree \(2010\)](#)]. Once hail stones reach a diameter where they cannot be vertically suspended by the updraft, they fall to the surface, passing through a layer of above-freezing air ([Nelson 1983](#)). The depth of this air, which is roughly quantified by the height of the environmental WBZ above ground, as well as the size of the hail stone itself, determines the amount of melting and the subsequent size of the stone when it reaches the surface ([Johns and Doswell 1992](#)).

These environmental characteristics, some of which can be considered ingredients (e.g., [Doswell and Schultz 2006](#)) for hail occurrence, vary in space and time and are often connected to the larger-scale extratropical circulation ([Johns and Doswell 1992](#); [Doswell et al. 1993](#); [Elsner and Widen 2014](#)). For example, environments favorable for hail formation, including those characterized by high CAPE and high vertical wind shear, are often found to the east of an eastward-moving upper-tropospheric trough and to the west of an upper-tropospheric ridge. Furthermore, this region is also synoptically favored for ascent due to upper-level divergence to the east of the trough. Regions to the south of a trough are also favored for hail formation, as here the height gradient increases upper-tropospheric winds and thus deep-layer shear. For a mean anticyclonic wind regime centered over the southeast United States, southerly 850-hPa winds would advect moisture and heat at low levels (given that moisture and heat increase to the south in the mean state), and westerly wind anomalies would be associated with faster flow speeds and a more favorable low-level wind shear regime for hail. However, it is important to note that this relationship is complex, as zonal flow, including flow that may be accelerated in response to a nearby ridge, may also favor severe storm development ([Mercer et al. 2012](#)). Regardless of the complexity, it is the teleconnected, intraseasonal modulation of upper-level circulation patterns by the tropical convection of the MJO that is of interest to the present study. For example, in the subtropics, ridges tend to amplify poleward of the eastward-moving positive MJO convective anomalies, while troughs tend to amplify poleward of the eastward-moving negative convective anomalies ([Roundy 2011](#)). These subtropical ridge and trough anomalies form wave trains that extend into the midlatitudes ([Hoskins and Karoly 1981](#); [Sardeshmukh and Hoskins 1988](#); [Jones et al. 2004](#)) that then affect local weather. For example, **TR13** found that an MJO-driven wave train yielded anomalous 300-hPa troughing over the western United States on March–May days with violent tornado outbreaks, and **BG13** found that it yielded anomalous 500-hPa troughing over the central United States on April–May central U.S. tornado days. This present study was motivated by a desire to extend results from both **TR13** and **BG13** to hail.

2. Data and methods

A hail-day climatology was developed for the contiguous United States for the period 1990–2013 in the following manner: first, all reports of hail of diameter at least 2.54 cm (1.00 in.) from the NOAA National Climatic Data Center (NCDC) database *Storm Data*

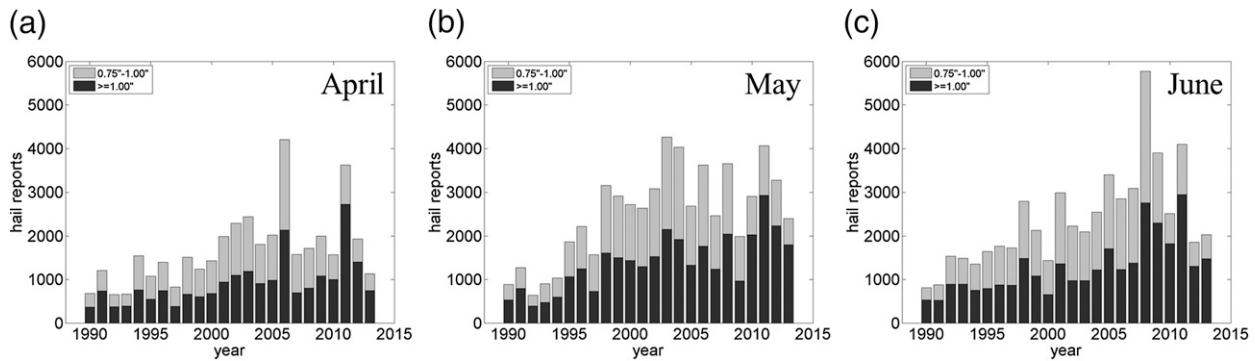


FIG. 1. Monthly hail reports in the United States for 1990–2013 from (a) April, (b) May, and (c) June. Black shading represents hail diameters ≥ 1.00 in., while gray represents hail with diameters ≥ 0.75 and ≤ 1.00 in. Total bar length represents total number of hail reports ≥ 0.75 in.

(available online at <http://www.spc.noaa.gov/wcm/>) for April, May, and June 1990–2013 were placed onto a 2° by 2° grid. Second, for each 2° by 2° grid box, days in which there was at least one 1-in. hail report somewhere in the grid box were classified as hail days, thereby forming a gridded hail-day dataset. Finally, daily frequency of hail for each month was calculated by dividing the number of hail days at each grid box by the number of days in the month. Hail diameter of 1.00 in. was chosen as a threshold because that diameter became the NWS operational lower limit for severe hail in 2010 (Ferree 2010); before 2010, the lower limit was 0.75 in. There are other known quantized biases in the record toward smaller diameters (Schaefer et al. 2004) and diameters of common objects like coins or sport equipment (Jewell and Brimelow 2009). For example, from 1990 to 2013, the number of reports of hail 1.90 cm (0.75 in.) and larger increased from around 1000 per year in April, May, and June to around 2000 per year in April and 3000 per year in May and June (Fig. 1). The number of reports of hail 2.54 cm (1.00 in.) also increased over the same period. Interestingly, in all three months, since 2010 when the NWS operational policy to define severe hail changed to only include hail of diameter 1.00 in. and larger, the ratio of reports of smaller hail to larger hail

decreased. This is potentially a result of smaller hail reports no longer being reported to the NWS or no longer being included in *Storm Data*. It is also potentially a result of bias toward the minimum severe threshold, particularly if severe reports are solicited in order to verify warnings. Users of *Storm Data* should be aware of this additional, recent artifact of the hail data record. Despite these changes in total number of hail reports per month, the number of hail days (where at least one hail report occurred somewhere in the country) remained nearly constant for April, May, and June (Fig. 2), with hail occurring on nearly every day in May and June for the 24-yr period. This gives us confidence in the reliability of this dataset for our analysis.

In addition to size bias, the *Storm Data* dataset has several other known biases. These include elevated numbers reports in urban areas compared to the immediate surroundings (Witt et al. 1998; Trapp et al. 2006), clustering of reports toward highways and road networks (Allen et al. 2015), and a general increase in the number of reports over the last 50 years (Schaefer et al. 2004). To mitigate the concern with the increase in hail reports, only hail reports from 1990 to 2013 were examined. To mitigate the concern about reports clustering around urban areas and rural infrastructure (e.g., road networks), reports were placed on

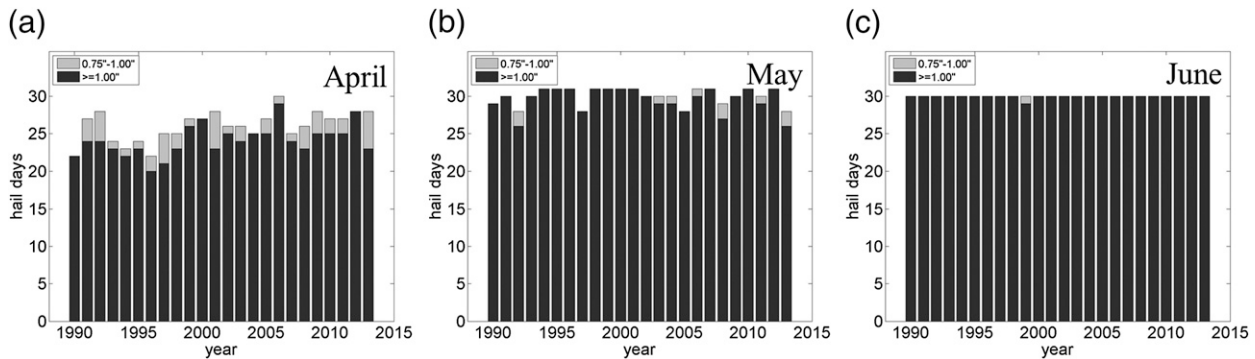


FIG. 2. Number of hail days (days with at least one hail report) in the United States from 1990 to 2013 for (a) April, (b) May, and (c) June. Dark and light shading is as in Fig. 1.

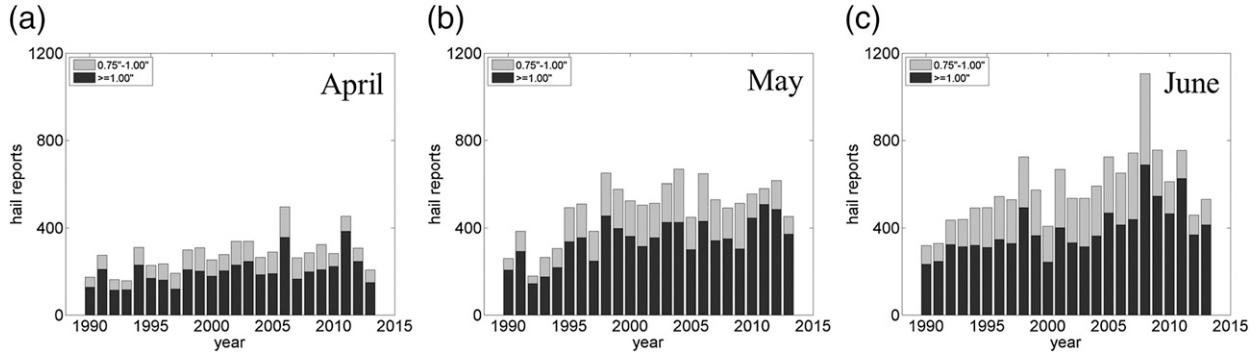


FIG. 3. Number of $2^\circ \times 2^\circ$ grid cells with hail days, 1990–2013, for (a) April, (b) May, and (c) June. Black shading represents counts of grids with hail days for hail with diameters ≥ 1.00 in., while gray represents hail with diameters ≥ 0.75 and ≤ 1.00 in. Total bar length represents total number of grid cells with hail of diameter ≥ 0.75 in.

a 2° by 2° grid (approximately 120 km by 120 km at 35°N). Finally, to mitigate the concern about quantization of sizes, only hail reports of 1.00 in. or greater were used. The total number of 0.75-in. and larger hail days on the grid increased between 1990 and 2013 (Fig. 3). When hail size was restricted to 1.00 in. and larger, the increase in gridded hail days was more muted, although still present (Fig. 3). Despite these concerns about data quality, the spatial distribution of monthly hail-day frequency (Fig. 4) resembled that of other climatologies [e.g., Doswell et al. (2005); Allen et al. (2015); and the operational SPC product], whereby hail frequency was highest in June, and the maximum hail frequency shifted north and west from April to June (Fig. 4). Magnitude of hail frequency was also similar to other climatologies, with a maximum hail-day frequency of 0.10–0.15 in May in central Oklahoma and Kansas that shifted to the high plains of Kansas and Colorado in June. A frequency of 0.10 means that there is a 10% chance of hail of at least 1.00-in. diameter in that grid box on that day. Thus, with 30 days in April, a grid box with hail-day frequency of 0.10 would expect to see, on average, 3 hail days in the month (Fig. 4). For urban areas with somewhat elevated frequencies relative to surrounding grid boxes, it is thought that any bias would be systematic, meaning that it would also appear when the data were filtered by phase of the MJO. Furthermore, this systematic bias should not be reflected in the environmental conditions. The eastern two-thirds of the United States was divided into four regions (Fig. 5) and Pearson product-moment correlation coefficients were calculated to quantify the strength of the relationships between hail-day and CAPE and shear anomalies in each of these regions.

The hail-day dataset was binned by phase of the MJO, determined using the Real-time Multivariate MJO (RMM) index (Wheeler and Hendon 2004). The RMM index is divided into eight phases that correspond to the general location of an MJO-enhanced equatorial

convective signal. Only active MJO days were considered for this study; an active MJO day was defined as one where the root sum of the two squared principal components, RMM1 and RMM2, was greater than 1, following the methodology of TR13 and BG13. Occurrences of each active MJO phase, as well as the inactive “neutral” phase, were counted to assess the distribution of MJO phases across the 13-week period (1 April–30 June) and the 24-yr period (1990–2013) (Figs. 6 and 7). While some variability was noted year to year, MJO phases were relatively evenly distributed from 1990 to 2013 (Fig. 6). However, more uneven distribution of MJO phases was found within each month (Fig. 7). For example, phases 3, 4, and 5 were common during the first week of April but largely absent during the last week of April; similarly, phases 1 and 2 were largely absent in the first week of April but were the most common phases during the last week. This variability had potential to bias the anomalies because of the change in hail-day frequency from the first to the last of the month. To mitigate this potential bias, hail-day frequencies were calculated for pentads instead of an entire month.

To retain the intraseasonal MJO signal in hail-day probabilities, no spatial or temporal smoothing was applied to the gridded hail-day data before it was binned by MJO phase. However, because of smaller sample size once the data were subdivided into pentads, smoothing was applied in the following manner. First, hail-day probabilities for each pentad were smoothed spatially using a 6° by 6° convolution kernel. Then, those spatially smoothed probabilities were smoothed in time using a 15-day Gaussian filter. Hail-day anomalies were calculated for each phase and pentad by subtracting the likelihood of a hail day during the neutral phase of MJO from the likelihood of a hail day for that particular MJO phase. Statistical significance was computed at each grid box for each pentad and MJO phase using a binary test. The z statistic in this test was calculated using

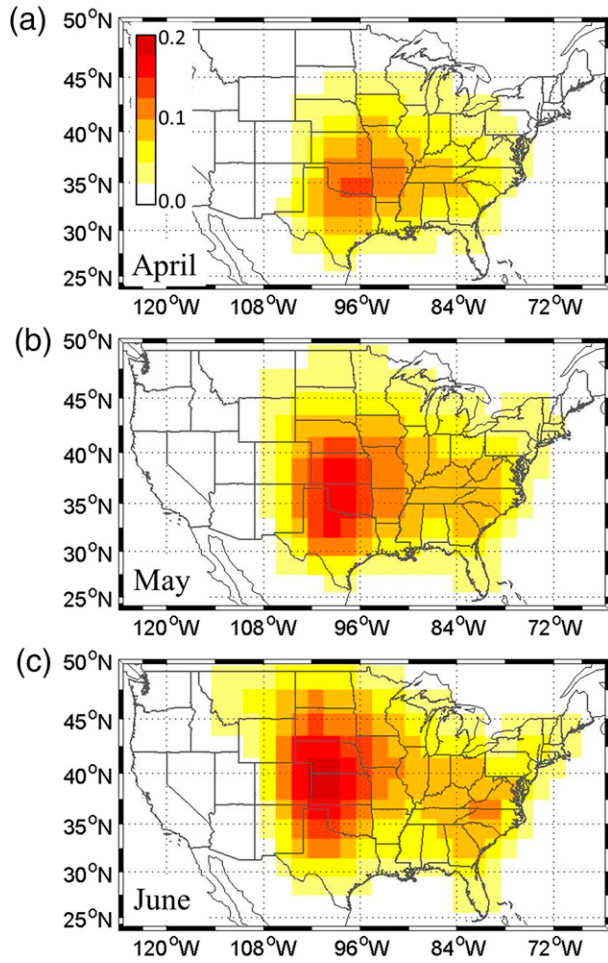


FIG. 4. Mean hail-day frequency for (a) April, (b) May, and (c) June, 1990–2013.

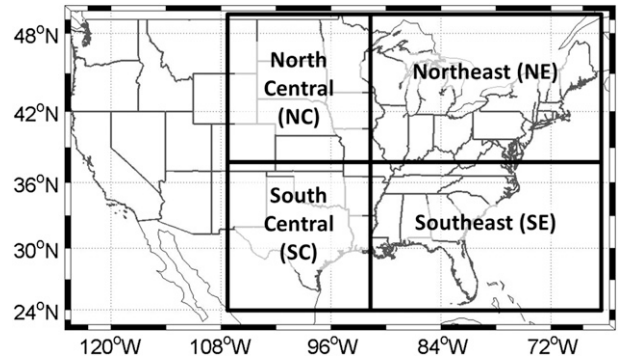


FIG. 5. Regional divisions referred to in the text.

(Knight and Knight 2001; Allen et al. 2011; Brooks 2013), were calculated for each MJO phase using the North American Regional Reanalysis (NARR; Mesinger et al. 2006). Composite anomalies of 300-hPa height and 850-hPa wind [from the NCEP–DOE AMIP-II Reanalysis; Kanamitsu et al. (2002)] were also calculated for each MJO phase to show variability of circulation by MJO phase. CAPE was obtained directly from the NARR archives, while 0–6-km bulk shear was found by vertically interpolating winds at constant pressure levels to above-ground level height coordinates following the methodology of Gensini and Ashley (2011). Surface-based CAPE was selected for this analysis over mean-layer CAPE because of the stronger correlation between surface-based CAPE and radiosonde observations (Gensini et al. 2014). In the NARR, surface-based CAPE has a known high bias (Gensini et al. 2014), thus in calculating the product of CAPE and S06 (hereafter called CS06), shear was given weight 1.67 (similar to Brooks 2013), giving $CS06 = CAPE \times S06^{1.67}$. Monthly climatologies of CS06 revealed maxima in eastern Texas and Oklahoma in April and May (Fig. 8). In June, the maximum of CS06 was located from eastern Kansas into Nebraska. Anomalies of CS06 were calculated at 2100 UTC for each MJO phase using the pentad-based method described above for hail days. Statistical significance of CS06 at each grid point was calculated using the Student's *t* test, and only those anomalies that were statistically significant at the 95% confidence level were considered. The 2100 UTC hour was chosen to sample the preconvective hail environment, as hail occurs most often in the hours around local sunset (Cecil and Blankenship 2012).

Anomalies of 300-hPa height and 850-hPa *u*- and *v*-wind components were calculated for each MJO phase using methodology similar to the hail-day anomalies. Height and wind anomalies were calculated by subtracting mean heights of the neutral phase from mean

where z_i is the *z* statistic for the *i*th phase of the MJO, \hat{p}_i is the probability of a hail day in the *i*th MJO phase, N_i is the total number of days in the *i*th MJO phase, and p_0 is the probability of a hail day in the neutral phase. Only hail-day anomalies with *p* values less than 0.05 were considered statistically significant. Statistically significant anomalies were combined equally to form a monthly mean. April hail-day anomalies thus comprised statistically significant anomalies for the pentads from 1 April to 30 April, May anomalies for the six pentads in May, and June anomalies for the six pentads in June.

Composite anomalies of the product of CAPE and magnitude of the 0–6-km vector wind difference (hereafter S06), variables known to be important for hail formation

$$z_i = \frac{\hat{p}_i - p_0}{p_0(1 - p_0)/\sqrt{N_i}},$$

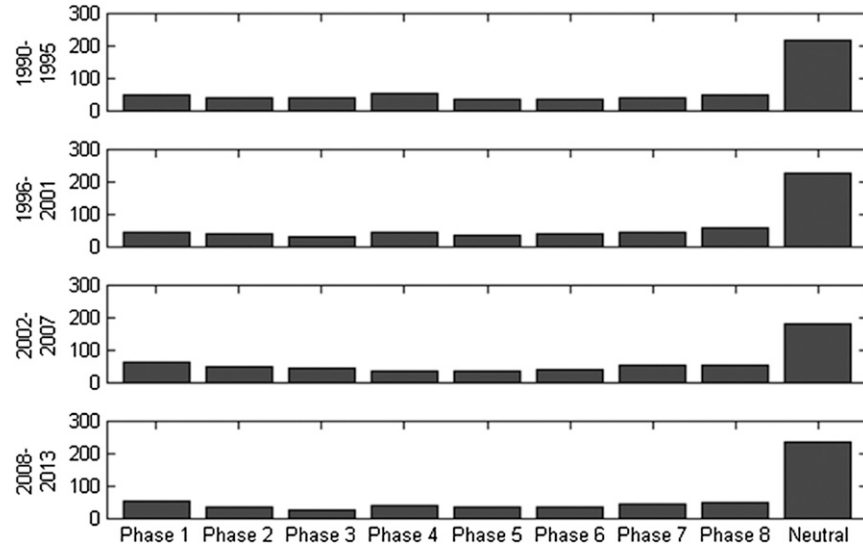


FIG. 6. Counts of MJO phase occurrence for RMM phases 1–8 for the 24-yr period, 1990–2013. Inactive MJO was classified as neutral.

heights for each MJO phase. Similar to hail-day anomalies, pentad anomalies of 300-hPa height and 850-hPa wind were calculated and then combined to form monthly anomalies. In April, mean 300-hPa heights were mostly zonal, with slight troughing over the southwest United States, and mean 850-hPa winds were anticyclonic, with southwesterly winds over much of the eastern and central United States (Fig. 8). In May, mean heights showed more of a trough over the western United States, centered farther west than in April. Mean 850-hPa winds were also anticyclonic, with southerly winds over the central United States and westerly winds over the northeastern United States. In June, mean 300-hPa heights featured a trough over the U.S. West Coast and a slight ridge of the central United States (Fig. 8). Mean 850-hPa winds were anticyclonic around an approximate center in the southeast United States. To provide global context to local height anomalies, composite height fields were assessed at lag periods from 0 to -15 days in a method similar to TR13. Finally, no spatial or temporal smoothing was applied to CS06, 850-hPa wind, or 300-hPa height anomalies.

3. Results

The primary findings of this MJO-hail analysis are as follows. First, hail-day frequency was found to vary by MJO phase in all three spring-season months. Second, many MJO phases featured dipolelike patterns in hail-day anomalies, indicating that in those phases, one region of the country would experience above-normal

probabilities of hail occurrence while another region of the country would experience below-normal probabilities of hail occurrence. Third, 850-hPa wind and 300-hPa geopotential height anomalies were often favorable for the observed hail-day anomalies. In many MJO phases, positive hail-day anomalies were often collocated with southerly or westerly 850-hPa wind anomalies and located east or south of negative 300-hPa height anomalies. Negative hail-day anomalies were often collocated with northerly or easterly 850-hPa wind anomalies and located east or south of positive height anomalies. Fourth, CS06 anomalies changed signs across different MJO phases, and in several phases, hail-day anomalies were strongly correlated with CS06 anomalies. Fifth, 300-hPa height anomalies at day 0 and backward to day -15 were part of a global wave train response to MJO convection, very similar to the results of Hoskins and Karoly (1981), Sardeshmukh and Hoskins (1988), and Matthews et al. (2004). When combined with the anomaly pattern in 850-hPa wind and 300-hPa height, the strong correlations between CS06 and hail-day anomalies indicate modulation of hail-day frequency by the MJO.

a. April

In April, a dipolelike pattern in hail-day anomalies was found in nearly every MJO phase (Fig. 9). For example, in phase 1, below-normal hail frequency was found over west Texas, Kansas, and eastward to Pennsylvania, while above-normal hail frequency was found over eastern Texas eastward to Alabama. In phases 5, 6, 7, and 8, positive hail-day anomalies were located

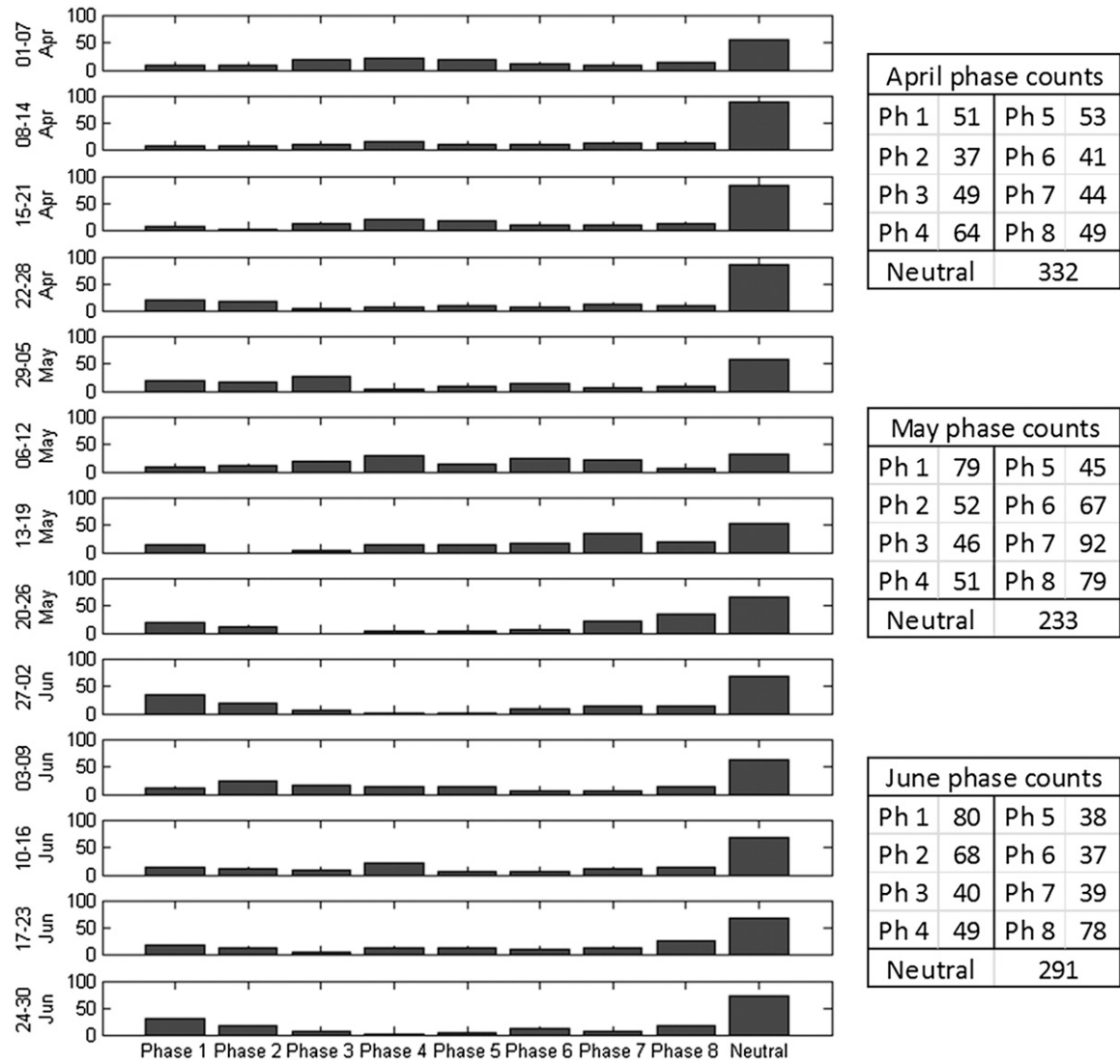


FIG. 7. Counts of each MJO phase occurrence for (left to right) RMM phases 1–8 for (top to bottom) the 13-week period of this study, 1 Apr–30 Jun. Inactive MJO was classified as neutral. Right-hand side tables show counts of each MJO phase occurrence per month.

generally over the south-central (SC) region. In phases 4 and 8, negative anomalies were located in the north-central (NC) and northeast (NE) regions. These hail-day anomalies ranged from -0.10 to $+0.08$, corresponding to increases (or decreases) of up to 125% of the monthly mean hail-day frequency (Fig. 4). Wind anomalies at 850 hPa were generally southerly or westerly in regions of positive hail-day anomalies and northerly or easterly in regions of negative hail-day anomalies (Fig. 9). Given the mean anticyclonic flow over much of the United States at 850 hPa (Fig. 8), southerly wind anomalies would be associated with favorable moisture and temperature advection, while westerly wind anomalies would be associated with a low-level shear pattern favorable for hail. At 300 hPa, height anomalies were present in every

MJO phase (Fig. 10). In phases 1, 2, and 3, positive hail-day anomalies were located east and south of negative height anomalies, in regions favorable for ascent and for greater deep-layer shear. In phases 4 and 8, negative hail-day anomalies [over the NC, SC, and NE in phase 4, and the NE and southeast (SE) in phase 8] were located west of negative height anomalies and east of positive height anomalies, and when superimposed on mean zonal flow (Fig. 8), these regions would be synoptically favored for descent. The SC region had the strongest correlations between hail-day and CS06, found in phase 5. Hail-day anomalies were strongly correlated to CS06 anomalies with a correlation coefficient of 0.88, and in that region, above-normal hail-day likelihood was found primarily in Kansas,

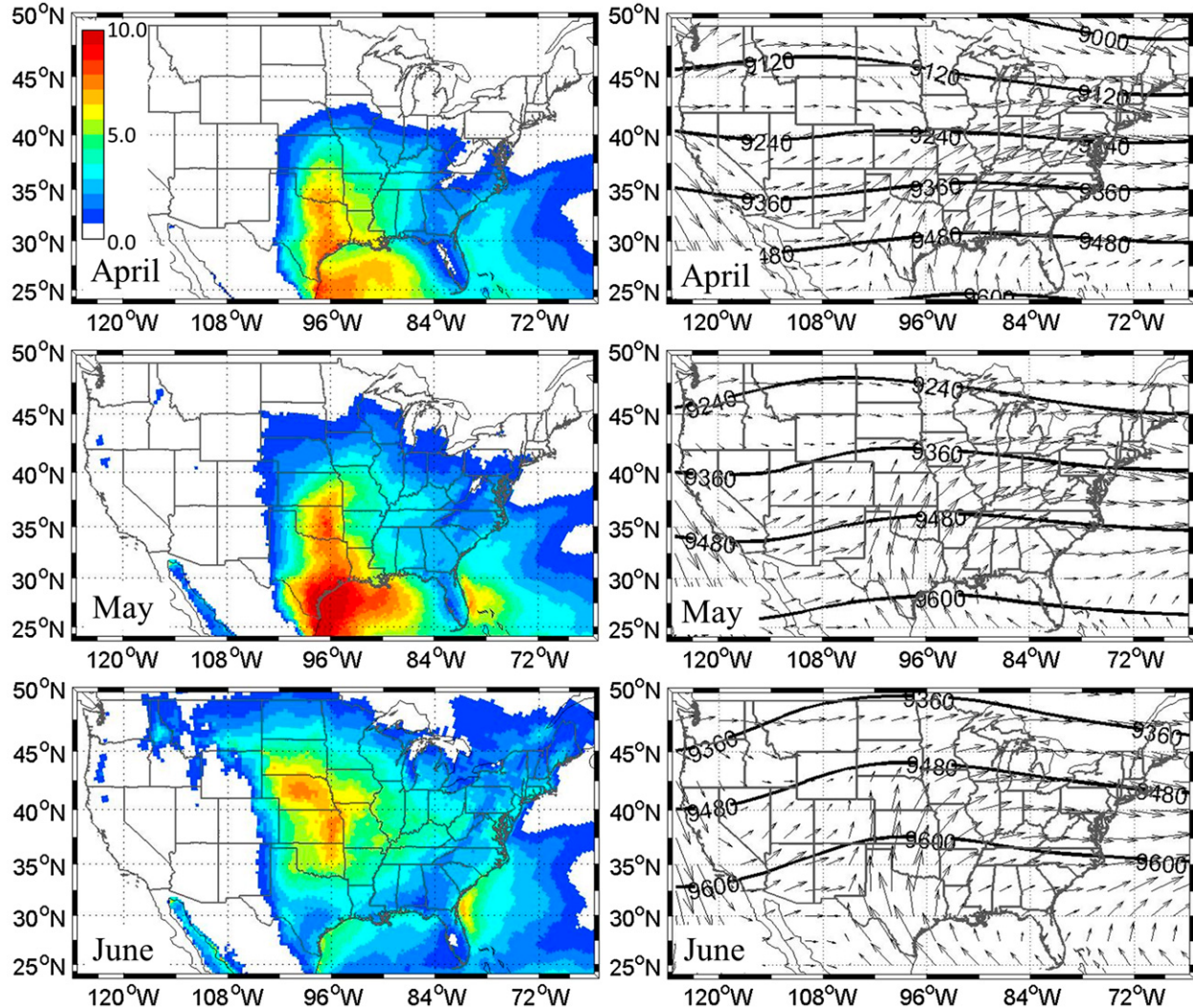


FIG. 8. (left) Mean CAPE times $S06^{1.67}$ (CS06; $m^3 s^{-3}$) scaled by 20 000, for (top to bottom) April, May, and June. (right) Mean 300-hPa height (m) and 850-hPa wind (relative speed and direction) for the same months.

Oklahoma, and Texas. Hail-day anomalies in the NC (phase 4) and NE (phase 2) regions were also highly correlated with CS06 (Table 1).

b. May

Similar to April, in May dipolelike patterns in the hail-day anomalies were found for many MJO phases, with phases 4 and 5 showing the clearest dipoles (Fig. 11). In phase 4, negative hail anomalies were located over the high plains, while positive hail anomalies were located farther east over eastern Oklahoma and Texas, Arkansas, and into the NE and SE. In phase 5, the dipole pattern was oriented more north-south, with positive hail anomalies stretching from Kansas and Nebraska eastward to Ohio, while negative hail anomalies were located along the Gulf Coast states. The dipolelike

structure suggests that the MJO's influence on hail occurs on the synoptic scale, and indeed the spatial separation between the two ends of the dipoles is approximately 1000 km, placing it in the middle of the range of synoptic-scale phenomena (Bluestein 1992). May hail-day anomalies by MJO phase varied from -0.15 to $+0.15$, which is as much as 100% of the monthly mean hail-day frequency (Fig. 4). The strongest correlations between CS06 and hail-day anomalies were found in the NE and NC regions during phase 3, with correlation coefficients of 0.90 and 0.80, respectively (Table 1). In the NC and SC regions, negative hail-day anomalies were collocated with negative CS06 anomalies and northerly 850-hPa wind anomalies (Fig. 11), both unfavorable for hail. Furthermore, the NC and SC regions were located over and west of up to -100 m 300-hPa

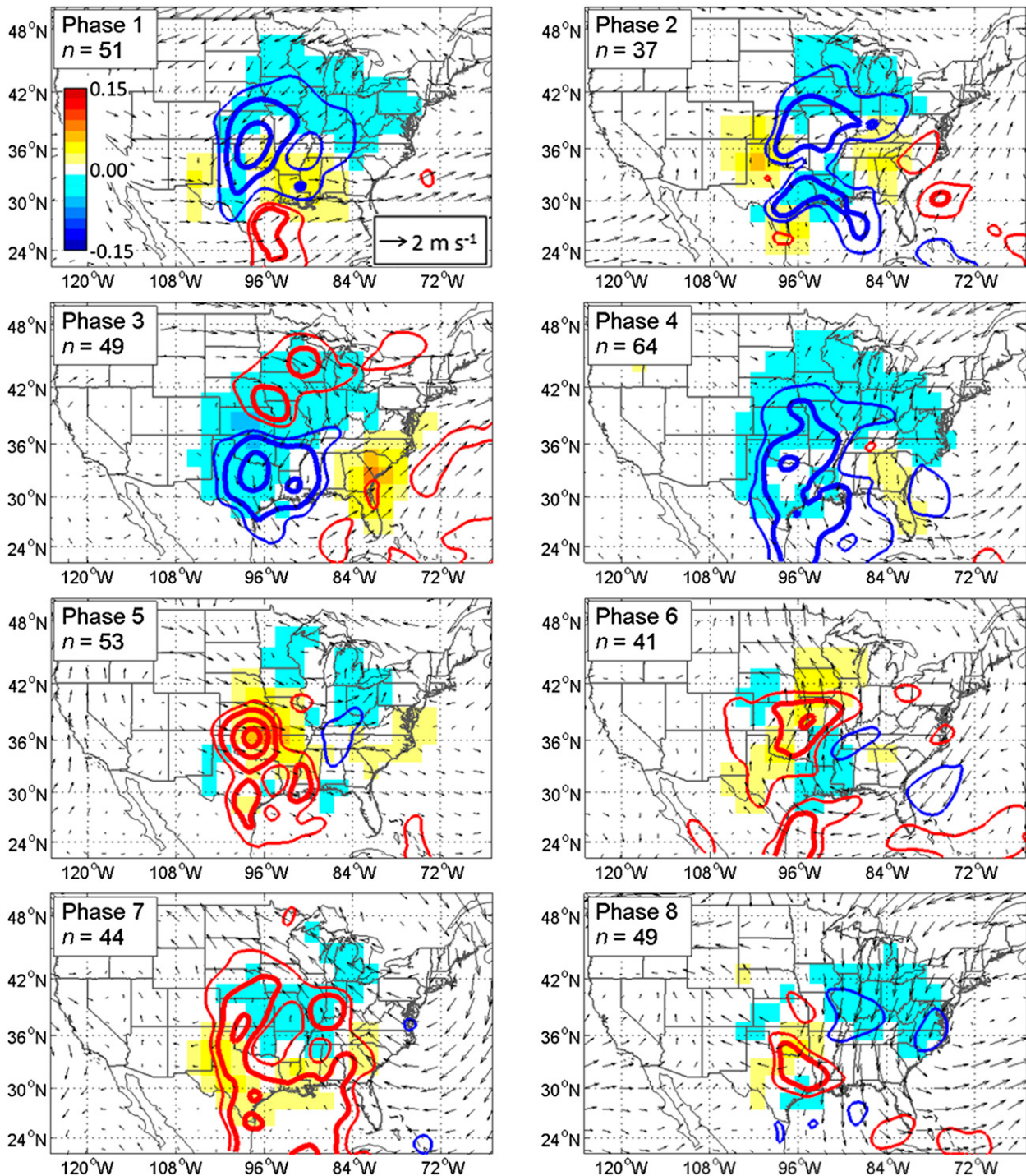


FIG. 9. April hail-day (day^{-1} ; shaded), 850-hPa wind vector, and CS06 ($\text{m}^3 \text{s}^{-3}$; red contour lines positive, blue contour lines negative; contour interval of 1.5) anomalies by MJO phase. Only anomalies of CS06 and hail that are statistically significant at the 95% level are shown.

height anomalies (Fig. 12), and given the background mean zonal flow over the eastern United States in May, negative height anomalies over the eastern United States would put the NC and SC regions in an area synoptically unfavorable for ascent.

c. June

In June, the strongest correlations between hail-day anomalies and CS06 anomalies were found in phase 2 over the northern plains, phase 5 over the southern and

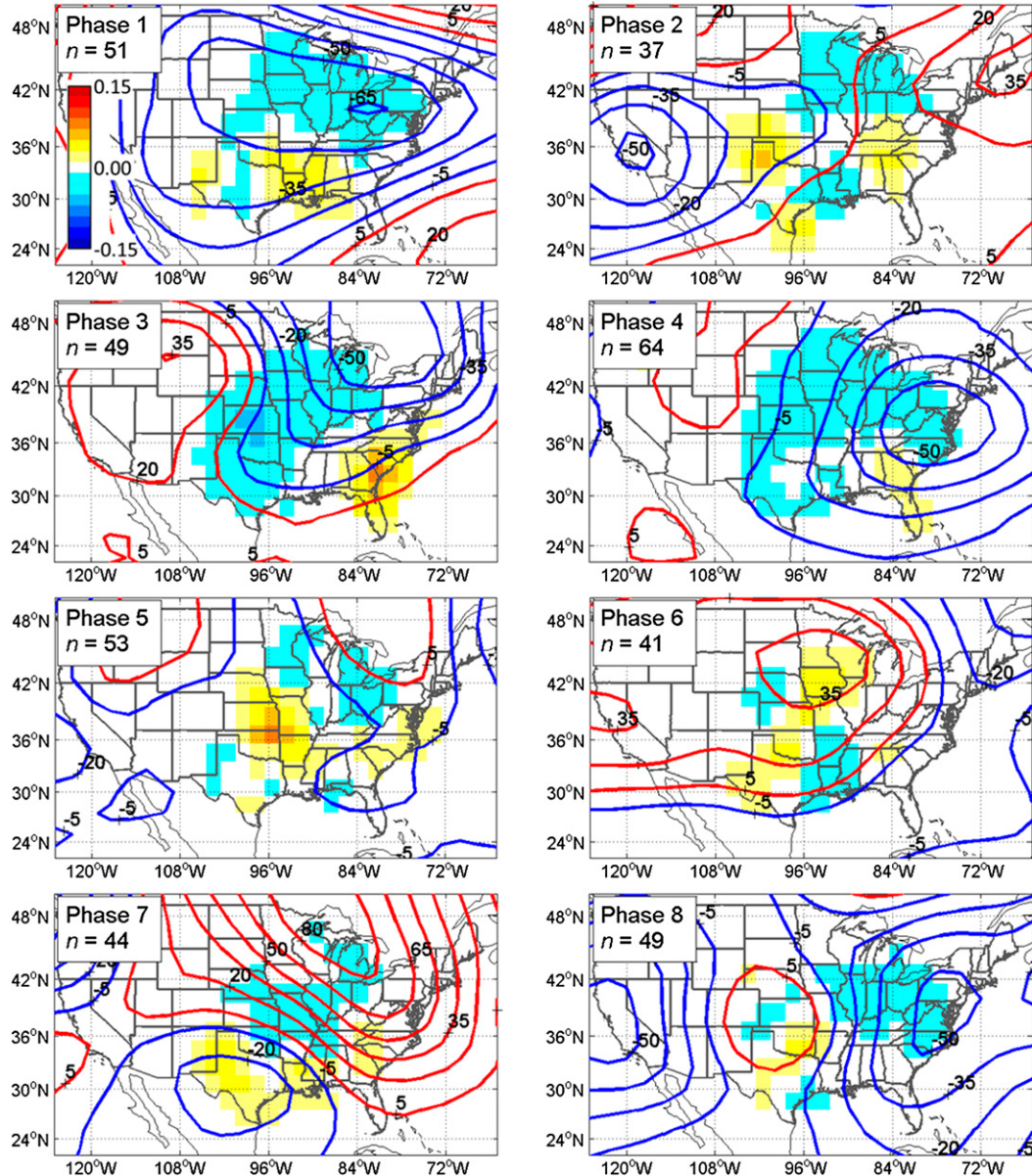


FIG. 10. As in Fig. 9, but for only hail-day anomalies plus 300-hPa height anomalies (m; red contour lines positive, blue contour lines negative).

central high plains, and phase 8 over much of the plains and Mississippi and Ohio River valleys (Fig. 13). In phase 2, positive hail-day anomalies from Kansas north to North Dakota were collocated with positive CS06 anomalies, with a correlation coefficient of 0.60. Westerly 850-hPa wind anomalies were found in the NC region, and when superimposed onto a westerly mean state (Fig. 8), provided enhanced low-level wind shear favorable for hail. In phase 8, negative hail-day anomalies over much of the eastern two-thirds of the United States were collocated with a large region of negative CS06 anomalies, yielding correlation

coefficients of 0.71, 0.88, and 0.71 for the SE, NE, and SC regions, respectively (Table 1). Here, 850-hPa wind anomalies were easterly or northerly, opposing the mean anticyclonic flow (Fig. 8), suggesting reduced moisture and heat advection in the region of below-normal hail activity. At 300 hPa, positive hail-day anomalies were found east of negative height anomalies (phases 2, 4, and 7), in areas synoptically favorable for ascent, and negative hail-day anomalies were found east of positive height anomalies (phases 1, 6, and 8), in areas synoptically unfavorable for ascent (Fig. 14).

TABLE 1. Pearson product-moment correlation coefficients between statistically significant hail anomalies and statistically significant CAPE times shear (CS06) anomalies. Bold font indicates the largest correlation coefficient for each region in each month. Region boundaries are defined in Fig. 5.

April				
	Southeast	Northeast	South-central	North-central
Phase 1	0.14	0.65	0.04	0.67
Phase 2	0.13	0.74	0.25	0.56
Phase 3	0.21	-0.62	0.60	-0.45
Phase 4	0.33	0.71	0.31	0.73
Phase 5	0.11	0.20	0.88	-0.20
Phase 6	0.05	0.43	0.17	-0.32
Phase 7	0.30	-0.28	0.28	-0.89
Phase 8	0.24	0.47	0.09	-0.19
May				
	Southeast	Northeast	South-central	North-central
Phase 1	-0.10	0.12	0.15	0.12
Phase 2	0.38	0.29	0.34	-0.51
Phase 3	0.02	0.90	0.44	0.80
Phase 4	0.36	0.50	0.55	0.61
Phase 5	0.33	0.31	-0.22	0.38
Phase 6	-0.06	0.11	-0.12	0.22
Phase 7	0.19	0.72	0.51	0.56
Phase 8	-0.03	-0.13	-0.11	0.25
June				
	Southeast	Northeast	South-central	North-central
Phase 1	0.29	0.68	0.39	0.15
Phase 2	-0.18	0.43	0.07	0.60
Phase 3	-0.28	-0.39	-0.35	0.07
Phase 4	0.16	0.40	-0.03	-0.04
Phase 5	0.12	-0.04	0.18	0.36
Phase 6	-0.19	-0.18	0.02	0.14
Phase 7	0.20	0.50	-0.01	0.06
Phase 8	0.71	0.87	0.71	0.35

d. Global context to regional variability

To assess the MJO's role in hail-day variability, it is important to examine global circulation anomalies (e.g., TR13). Here, only phase 1 in April is presented, but all phases and months were found to behave similarly, with global wave trains evolving over the 15-day period leading up to the particular MJO phase. At days -15 and -12, positive height anomalies were located over central North America and neutral height anomalies were located over northern North America (Fig. 15). By days -9 and -6, positive heights built over northern North America and the trough over Japan at day -12 shifted east and deepened between Japan and Alaska. Furthermore, at these lags, height anomalies more closely resembled a wave train, with ridging over northern North America and northern Eurasia and troughing over Europe and East Asia. Downstream of this trough, ridging was present over northern Canada.

By days -3 and 0 (in this case, day 0 corresponded to MJO phase 1), ridging over northern Canada had amplified (to anomalies of up to +150 m), resulting in negative height anomalies (about -60 m) centered downstream over the eastern and central United States (Fig. 15).

The establishment of this wavy pattern by day 0 is a defining characteristic of the MJO (Zhang 2005). Including 850-hPa wind and CS06 anomalies, we see that the MJO's influence was not limited to the upper troposphere. Thus, as large-scale upper-level circulation anomalies evolve with the MJO, they both project onto smaller-scale phenomena, including lower-troposphere wind and local buoyancy and shear, and also themselves provide large-scale support for convective storm activity.

4. Discussion and conclusions

The results of this study provide a better understanding of the interaction between planetary-scale phenomena, such as the Madden-Julian oscillation, and synoptic- and mesoscale phenomena, such as hail-producing thunderstorms. Based on the patterns seen in hail-day, CS06, 850-hPa wind, and 300-hPa height anomalies, if the MJO's impact on hail is seen via a downscale response: different phases of the MJO modulate synoptic-scale circulation across the United States, and these circulation anomalies lead to synoptic-scale circulation favorable (or unfavorable, for the case of negative hail-day anomalies) for hail-producing convective storms. Different phases of the MJO are also associated with mesoscale conditions favorable for severe convective storms: increased buoyancy (CAPE) and deep-layer shear (S06), whose anomalies are consequences of the modulated synoptic-scale circulation. Dipolelike structures in hail-day anomalies were seen in April, May, and June. The distance between positive and negative anomaly centers was synoptic scale, providing evidence for the modulation of background state on the synoptic scale.

These results somewhat agree with recent work connecting the MJO to tornado activity. For example, BG13 found tornado days to be most frequent in phase 8 in April and phase 5 in May. In this study, in April during phase 8, we found positive CS06 and hail-day anomalies extending from central Texas north into Oklahoma, and in May, we found positive hail-day and CS06 anomalies extending over a large region from northern Oklahoma to Nebraska and east to Tennessee, Kentucky, and Ohio. Additionally, TR13 found tornado outbreaks to be most common from March to May during phase 2, and in April, we found regions of positive hail-day anomalies during phase 2 in agreement with TR13. However, during May's phase 2, we found mostly

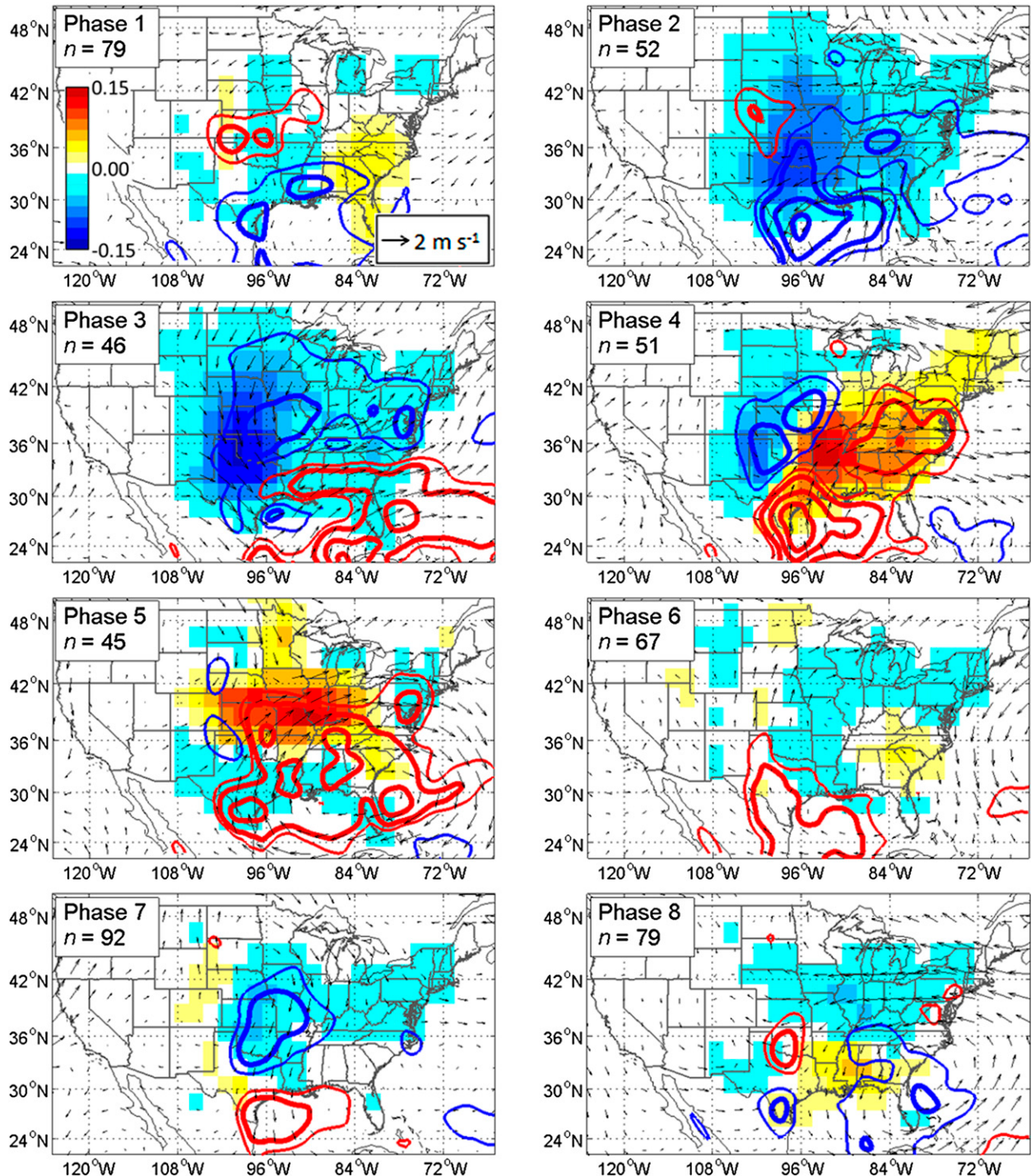


FIG. 11. As in Fig. 9, but for May.

negative hail-day and CS06 anomalies, and these were collocated with east and northeast 850-hPa wind anomalies. At 300-hPa, subtle differences between TR13 and May's phase 2 were noted. For example, the negative height anomaly in TR13 was centered over Utah and

Colorado, farther east and north than the negative height anomaly in May's phase 2 of the current study that was centered over southern California and into the Pacific. Furthermore, the positive height anomaly in TR13 was centered over North Carolina, while in May's phase 2 of

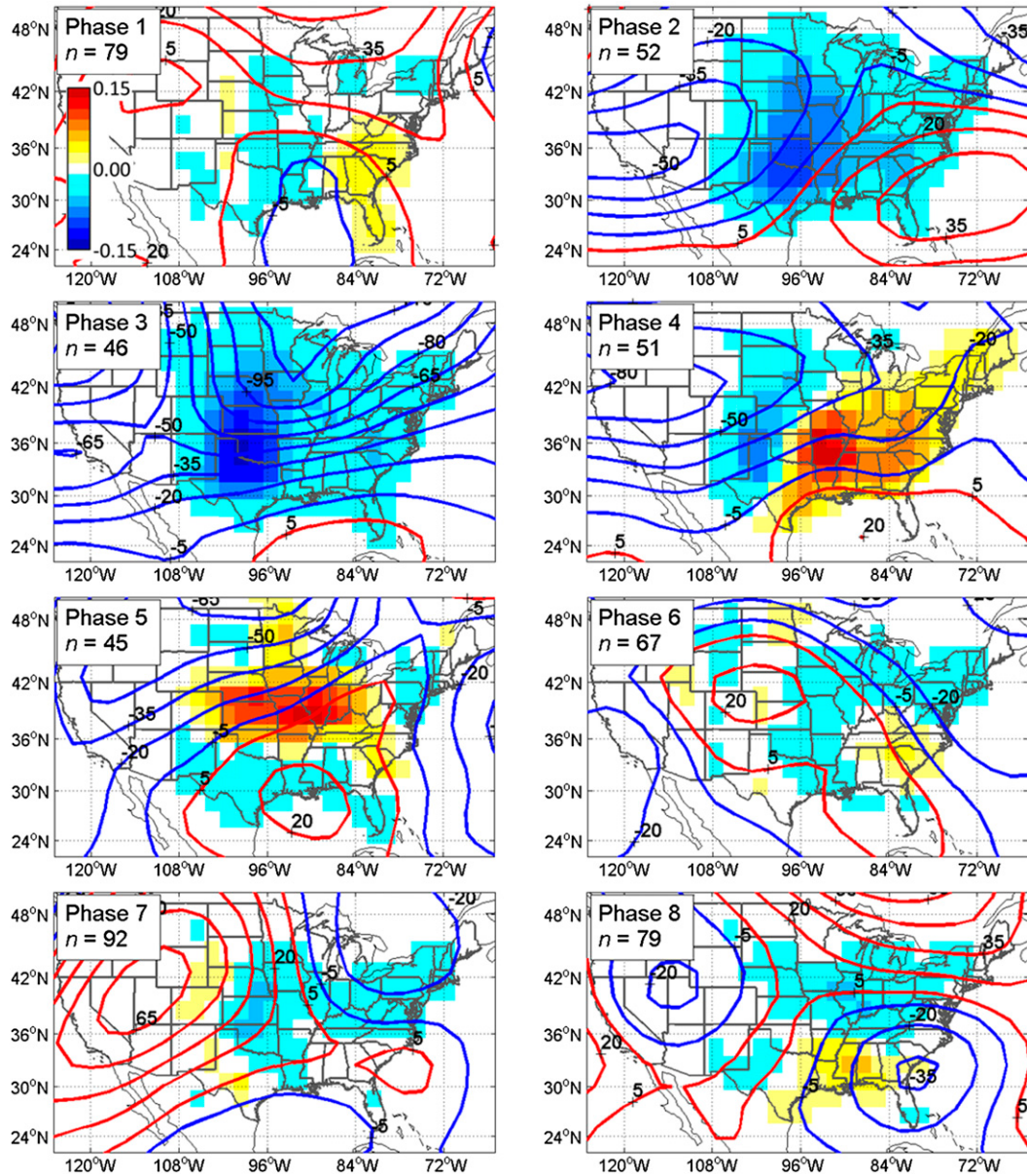


FIG. 12. As in Fig. 10, but for May.

the current study, it was centered over the Atlantic Ocean to the southeast of the SE region. In May, the 300-hPa height pattern that most closely resembled TR13 appeared in phase 4.

There are several important limitations to these results. First, as discussed in section 2, the hail record in *Storm Data* contains nonmeteorological influences, including an increase in the number of reports over the study period (Fig. 2) and the clustering of reports near cities and the road network. While the latter (clustering of reports) is likely to be at least somewhat mitigated by the 2° by 2° grid size, the former (increase in reports) still

remains a concern. Additionally, while the MJO is generally evenly distributed across each 6-yr period of the 24-yr study (Fig. 6), the phase distribution is not as evenly distributed within a month (Fig. 7). While pentad averaging was used to reduce this bias, it is possible that some of the weak or negative correlations between CS06 and hail-day anomalies could be due to this uneven distribution of MJO phase occurrence. Additionally, while other studies have drawn meaningful conclusions about intraseasonal variability using shorter time periods than 24 years, it is known that circulation patterns and hail formation are controlled by other factors besides the

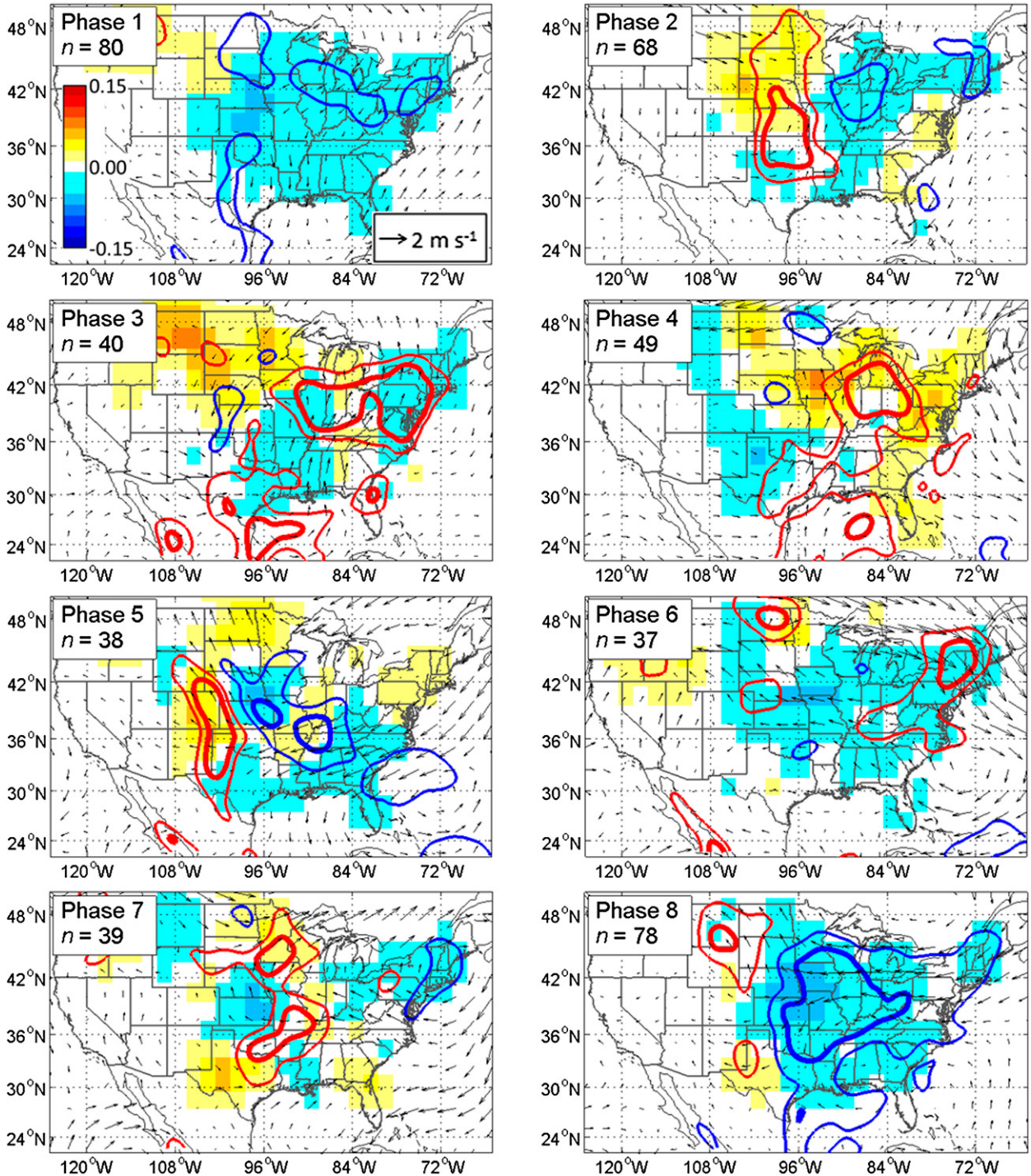


FIG. 13. As in Figs. 9, but for June.

MJO, including other natural modes of climate variability. The RMM index does remove the interseasonal signal, but a known flaw is that it captures all tropical convection, including cloud clusters not associated with the MJO (Ventrice et al. 2013). Furthermore, the

synoptic circulation pattern favorable for hail is more complex than a simple ridge-trough couplet (Doswell et al. 2006; Shafer et al. 2009, 2010). For example, Mercer et al. (2012) showed that the upper-level flow in severe events with only hail and damaging wind (and not

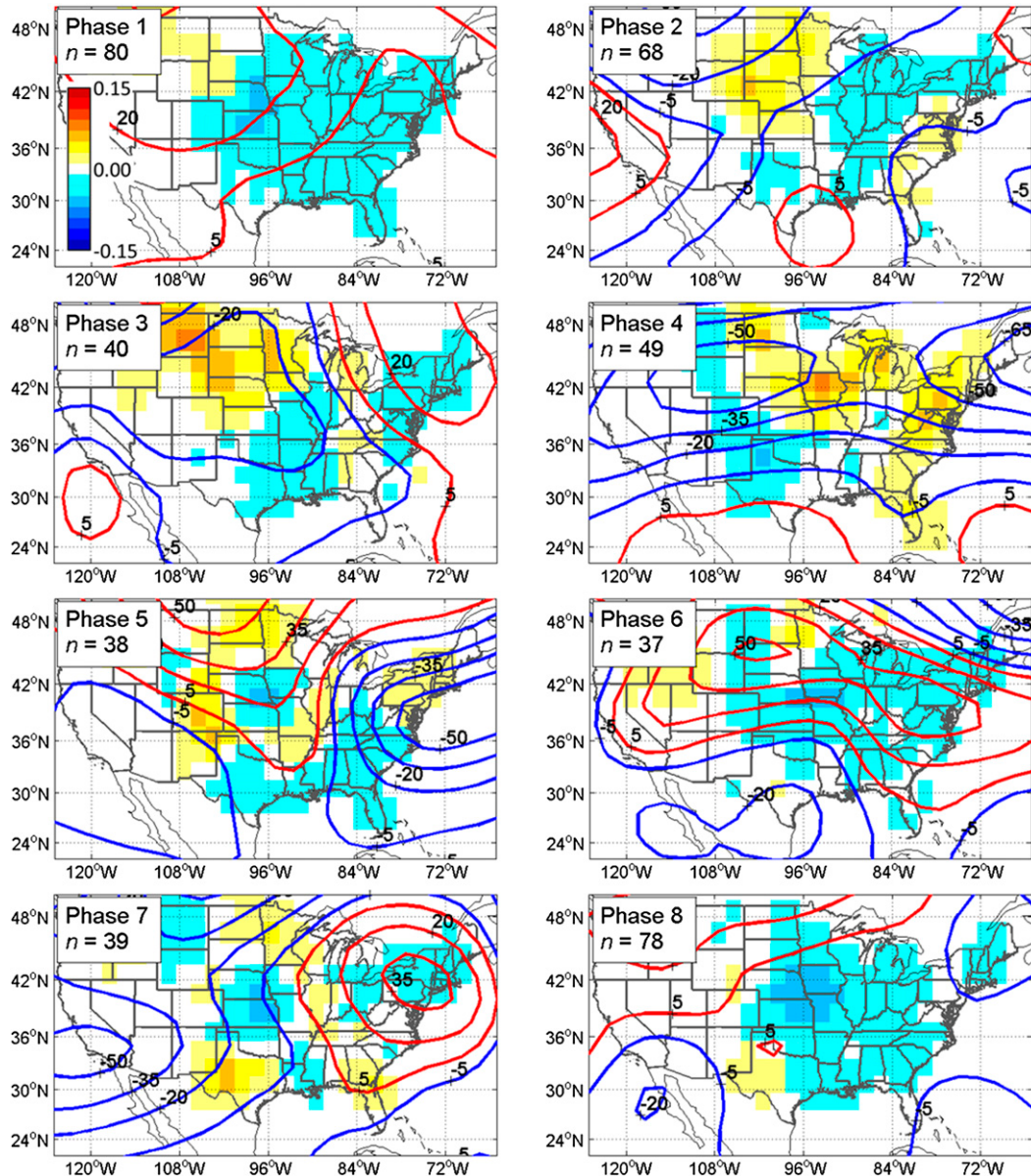


FIG. 14. As in Figs. 10, but for June.

tornadoes) was relatively zonal. This suggests that the general height patterns in Figs. 10, 12, and 14 may not have been as favorable or unfavorable for hail as the sign of the anomaly might otherwise suggest. Finally, not every favorable hail environment yields hail observations, and furthermore, some hail environments, including those at night or early morning are probably poorly correlated with CS06 at 2100 UTC.

Despite these concerns, each month featured several MJO phases where anomalies of hail days and atmospheric fields were strongly positively correlated. Maximum correlation coefficients of 0.88 in April (phase 5 in the SC region), 0.90 in May (phase 3 in the NE region),

and 0.87 in June (phase 8 in the SC region) were found. These results indicate a robust statistical link between hail occurrence and the MJO. The physical link comes from the globally evolving height field, which in turn modifies the background state circulation over the United States and leads to local environmental conditions favoring hail. We suggest that future work on this topic cluster in two areas: prediction and understanding. Skillful MJO predictability is now possible beyond 27 days in the coupled ECMWF (VarEPS) prediction system and beyond 21 days in the coupled NCEP (CFSv2) prediction system (Kim et al. 2014). Thus, additional studies such as this one that statistically connect the

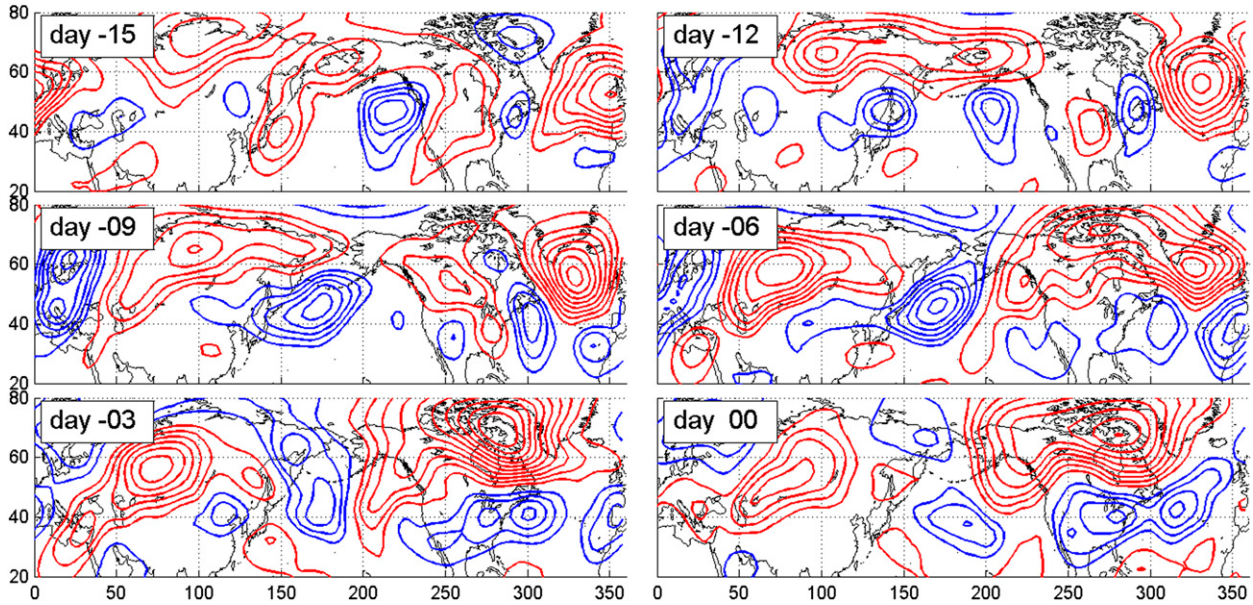


FIG. 15. Lagged 300-hPa height anomalies for April phase 1. Red (blue) curves represent positive (negative) height anomalies. The contour interval for both sets of curves is 30 m.

MJO to mesoscale weather events are needed to improve predictability of midlatitude extreme weather at lead times beyond 4 or 5 days (e.g., Jones et al. 2011). To this end, in 2014, the NOAA Storm Prediction Center (SPC), in collaboration with the Cooperative Institute for Mesoscale Meteorological Studies (CIMMS), is currently embarking on an effort to extend prediction of severe outbreaks beyond the current operational 8-day window (see <http://wiki.iri.columbia.edu/index.php?n=Climate.TornadoWorkshop>). In the synoptic-scale time window (0–7 days), it is critical to understand all of the modes of variability that may be contributing to an observed circulation pattern. Thus, additional work is needed to further the understanding of multiscale interactions between the tropics and extratropics.

Acknowledgments. This work was partially supported by NSF Grant AGS-1240143. The authors thank V. Gensini for providing gridded 0–6-km shear data from the NARR. The authors thank S. Mrose-Boles of the Science and Engineering Apprenticeship Program (SEAP) and H. Leslie for providing helpful edits to the manuscript. Finally, the authors thank the anonymous reviewers for their helpful comments and suggestions.

REFERENCES

- Allen, J. T., D. J. Karoly, and G. A. Mills, 2011: A severe thunderstorm climatology for Australia and associated thunderstorm environments. *Aust. Meteor. Ocean J.*, **61**, 143–158.
—, M. K. Tippett, and A. H. Sobel, 2015: An empirical model relating U.S. monthly hail occurrence to large-scale meteorological environment. *J. Adv. Model. Earth Syst.*, doi:[10.1002/2014MS000397](https://doi.org/10.1002/2014MS000397), in press.
Barrett, B. S., and V. A. Gensini, 2013: Variability of central United States April–May tornado day likelihood by phase of the Madden-Julian Oscillation. *Geophys. Res. Lett.*, **40**, 2790–2795, doi:[10.1002/grl.50522](https://doi.org/10.1002/grl.50522).
Bluestein, H. B., 1992: *Principles of Kinematics and Dynamics. Vol. 1, Synoptic-Dynamic Meteorology in Midlatitudes*, Oxford University Press, 448 pp.
Brandes, E., J. Vivekanandan, J. Tuttle, and G. Kessinger, 1997: Hail production in Northeast Colorado hailstorms. Preprints, 27th Conf. on Radar Meteorology, Vail, CO, Amer. Meteor. Soc., 527–530.
Brooks, H. E., 2013: Severe thunderstorms and climate change. *Atmos. Res.*, **123**, 129–138, doi:[10.1016/j.atmosres.2012.04.002](https://doi.org/10.1016/j.atmosres.2012.04.002).
—, and R. B. Wilhelmson, 1990: The effects of low-level hodograph curvature on supercell structure. Preprints, 16th Conf. on Severe Local Storms, Kananaskis Park, Alberta, Canada, Amer. Meteor. Soc., 34–39.
Browning, K. A., 1977: The structure and mechanisms of hailstorms. *Hail: A Review of Hail Science and Hail Suppression*, Meteor. Monogr., No. 38, Amer. Meteor. Soc., 1–43.
Cecil, D. J., and C. B. Blankenship, 2012: Toward a global climatology of severe hailstorms as estimated by satellite passive microwave imagers. *J. Climate*, **25**, 687–703, doi:[10.1175/JCLI-D-11-00130.1](https://doi.org/10.1175/JCLI-D-11-00130.1).
Changnon, S. A., 1999: Data and approaches for determining hail risk in the contiguous United States. *J. Appl. Meteor.*, **38**, 1730–1739, doi:[10.1175/1520-0450\(1999\)038<1730:DAAFDH>2.0.CO;2](https://doi.org/10.1175/1520-0450(1999)038<1730:DAAFDH>2.0.CO;2).
—, 2002: Climatology of hail risk in the United States. Tech. Rep. CRR-40, Changnon Climatologists, Mahomet, IL, 67 pp.
—, and D. Changnon, 2009: Assessment of a method used to time-adjust past storm losses. *Nat. Hazards*, **38**, 4–12.
—, —, and S. D. Hilberg, 2009: Hailstorms across the nation: An atlas about hail and its damages. Illinois State Water Survey Contract Rep. 2009-12, 101 pp.

- Cintineo, J. L., T. M. Smith, V. Lakshmanan, H. E. Brooks, and K. L. Ortega, 2012: An objective high-resolution hail climatology of the contiguous United States. *Wea. Forecasting*, **27**, 1235–1248, doi:[10.1175/WAF-D-11-00151.1](https://doi.org/10.1175/WAF-D-11-00151.1).
- Doswell, C. A., III, and D. M. Schultz, 2006: On the use of indices and parameters in forecasting. *Electron. J. Severe Storms Meteor.*, **1** (3). [Available online at <http://www.ejssm.org/ojs/index.php/ejssm/article/viewArticle/11/12>.]
- , S. J. Weiss, and R. H. Johns, 1993: Tornado forecasting: A review. *The Tornado: Its Structure, Dynamics, Prediction, and Hazards, Geophys. Monogr.*, Vol. 79, Amer. Geophys. Union, 557–571.
- , H. E. Brooks, and M. P. Kay, 2005: Climatological estimates of daily local nontornadic severe thunderstorm probability for the United States. *Wea. Forecasting*, **20**, 577–595, doi:[10.1175/WAF866.1](https://doi.org/10.1175/WAF866.1).
- , R. Edwards, R. L. Thompson, J. A. Hart, and K. C. Crosbie, 2006: A simple and flexible method for ranking severe weather events. *Wea. Forecasting*, **21**, 939–951, doi:[10.1175/WAF959.1](https://doi.org/10.1175/WAF959.1).
- Douglas, R. H., 1963: Recent hail research: A review. *Severe Local Storms, Meteor. Monogr.*, No. 27, Amer. Meteor. Soc., 157–172.
- Elsner, J. B., and H. M. Widen, 2014: Predicting spring tornado activity in the central Great Plains by 1 March. *Mon. Wea. Rev.*, **142**, 259–267, doi:[10.1175/MWR-D-13-00014.1](https://doi.org/10.1175/MWR-D-13-00014.1).
- Emersic, C., P. L. Heinselman, D. R. MacGorman, and E. C. Bruning, 2011: Lightning activity in a hail-producing storm observed with phased-array radar. *Mon. Wea. Rev.*, **139**, 1809–1825, doi:[10.1175/2010MWR3574.1](https://doi.org/10.1175/2010MWR3574.1).
- Ferree, J., 2010: National change of the hail criteria for severe storms from 3/4 inch to 1 inch beginning January 5, 2010. Severe Storms Services, NOAA/National Weather Service, 8 pp. [Available online at http://www.nws.noaa.gov/oneinchhail/docs/One_Inch_Hail.pdf].
- Foote, G. B., and C. A. Knight, Eds., 1977: *Hail: A Review of Hail Science and Hail Suppression*. Meteor. Monogr., No. 38, Amer. Meteor. Soc., 277 pp.
- Gensini, V. A., and W. S. Ashley, 2011: Climatology of potentially severe convective environments from the North American Regional Reanalysis. *Electron. J. Severe Storms Meteor.*, **6** (8). [Available online at <http://www.ejssm.org/ojs/index.php/ejssm/article/viewArticle/85>.]
- , T. L. Mote, and H. E. Brooks, 2014: Severe thunderstorm reanalysis environments and collocated radiosonde observations. *J. Appl. Meteor. Climatol.*, **53**, 742–751, doi:[10.1175/JAMC-D-13-0263.1](https://doi.org/10.1175/JAMC-D-13-0263.1).
- Hoskins, B. J., and D. J. Karoly, 1981: The steady linear response of a spherical atmosphere to thermal and orographic forcing. *J. Atmos. Sci.*, **38**, 1179–1196, doi:[10.1175/1520-0469\(1981\)038<1179:TSRLOA>2.0.CO;2](https://doi.org/10.1175/1520-0469(1981)038<1179:TSRLOA>2.0.CO;2).
- Hughes, P., and R. Wood, 1993: Hail: The white plague. *Weatherwise*, **46**, 16–21, doi:[10.1080/00431672.1993.9930228](https://doi.org/10.1080/00431672.1993.9930228).
- Jewell, R., and J. Brimelow, 2009: Evaluation of Alberta hail growth model using severe hail proximity soundings from the United States. *Wea. Forecasting*, **24**, 1592–1609, doi:[10.1175/2009WAF2222230.1](https://doi.org/10.1175/2009WAF2222230.1).
- Johns, R. H., and C. A. Doswell III, 1992: Severe local storms forecasting. *Wea. Forecasting*, **7**, 588–612, doi:[10.1175/1520-0434\(1992\)007<0588:SLSF>2.0.CO;2](https://doi.org/10.1175/1520-0434(1992)007<0588:SLSF>2.0.CO;2).
- Jones, C., D. E. Waliser, K. M. Lau, and W. Stern, 2004: The Madden-Julian Oscillation and its impact on Northern Hemisphere weather predictability. *Mon. Wea. Rev.*, **132**, 1462–1471, doi:[10.1175/1520-0493\(2004\)132<1462:TMOAI>2.0.CO;2](https://doi.org/10.1175/1520-0493(2004)132<1462:TMOAI>2.0.CO;2).
- , J. Gottschalck, L. Carvalho, and W. Higgins, 2011: Influence of the Madden-Julian oscillation on forecasts of extreme precipitation in the contiguous United States. *Mon. Wea. Rev.*, **139**, 332–350, doi:[10.1175/2010MWR3512.1](https://doi.org/10.1175/2010MWR3512.1).
- Kanamitsu, M., W. Ebisuzaki, J. Woollen, S.-K. Yang, J. J. Hnilo, M. Fiorino, and G. L. Potter, 2002: NCEP–DOE AMIP-II Reanalysis (R-2). *Bull. Amer. Meteor. Soc.*, **83**, 1631–1643, doi:[10.1175/BAMS-83-11-1631](https://doi.org/10.1175/BAMS-83-11-1631).
- Kim, H.-M., P. J. Webster, V. E. Toma, and D. Kim, 2014: Predictability and prediction skill of the MJO in two operational forecasting systems. *J. Climate*, **27**, 5364–5378, doi:[10.1175/JCLI-D-13-00480.1](https://doi.org/10.1175/JCLI-D-13-00480.1).
- Knight, C. A., and N. C. Knight, 2001: Hailstorms. *Severe Convective Storms, Meteor. Monogr.*, No. 50, Amer. Meteor. Soc., 223–254.
- Madden, R., and P. Julian, 1972: Description of global-scale circulation cells in the tropics with a 40–50 day period. *J. Atmos. Sci.*, **29**, 1109–1123, doi:[10.1175/1520-0469\(1972\)029<1109:DGSCC>2.0.CO;2](https://doi.org/10.1175/1520-0469(1972)029<1109:DGSCC>2.0.CO;2).
- Matthews, A. J., B. J. Hoskins, and M. Masutani, 2004: The global response to tropical heating in the Madden-Julian Oscillation during Northern winter. *Quart. J. Roy. Meteor. Soc.*, **130**, 1991–2011, doi:[10.1256/qj.02.123](https://doi.org/10.1256/qj.02.123).
- McCaul, W. W., Jr., 1990: Simulations of convective storms in hurricane environments. Preprints, *16th Conf. on Severe Local Storms*, Kananaskis Park, Alberta, Canada, Amer. Meteor. Soc., 334–339.
- Mercer, A. E., C. M. Shafer, C. A. Doswell, L. M. Leslie, and M. B. Richman, 2012: Synoptic composites of tornadic and non-tornadic outbreaks. *Mon. Wea. Rev.*, **140**, 2590–2608, doi:[10.1175/MWR-D-12-00029.1](https://doi.org/10.1175/MWR-D-12-00029.1).
- Mesinger, F., and Coauthors, 2006: North American Regional Reanalysis. *Bull. Amer. Meteor. Soc.*, **87**, 343–360, doi:[10.1175/BAMS-87-3-343](https://doi.org/10.1175/BAMS-87-3-343).
- Nelson, S. P., 1983: The influence of storm flow structure on hail growth. *J. Atmos. Sci.*, **40**, 1965–1983, doi:[10.1175/1520-0469\(1983\)040<1965:TIOSFS>2.0.CO;2](https://doi.org/10.1175/1520-0469(1983)040<1965:TIOSFS>2.0.CO;2).
- Roundy, P. E., 2011: Tropical extratropical interactions. *Intra-seasonal Variability in the Atmosphere-Ocean Climate System*, 2nd ed. W. K. M. Lau and D. E. Waliser, Eds., Springer, 497–512.
- Ryzhkov, A. V., M. R. Kumjian, S. M. Ganson, and A. P. Khain, 2013: Polarimetric radar characteristics of melting hail. Part I: Theoretical simulations using spectral microphysical modeling. *J. Appl. Meteor. Climatol.*, **52**, 2849–2870, doi:[10.1175/JAMC-D-13-073.1](https://doi.org/10.1175/JAMC-D-13-073.1).
- Sardeshmukh, P. D., and B. J. Hoskins, 1988: The generation of global rotational flow by steady idealized tropical divergence. *J. Atmos. Sci.*, **45**, 1228–1251, doi:[10.1175/1520-0469\(1988\)045<1228:TGORFR>2.0.CO;2](https://doi.org/10.1175/1520-0469(1988)045<1228:TGORFR>2.0.CO;2).
- Schafer, J. T., J. J. Levit, S. J. Weiss, and D. W. McCarthy, 2004: The frequency of large hail over the contiguous United States. *14th Conf. on Applied Meteorology*, Seattle, WA, Amer. Meteor. Soc., 3.3. [Available online at <http://ams.confex.com/ams/pdfpapers/69834.pdf>.]
- Shafer, C. M., A. E. Mercer, C. A. Doswell, M. B. Richman, and L. M. Leslie, 2009: Evaluation of WRF forecasts of tornadic and nontornadic outbreaks when initialized with synoptic-scale input. *Mon. Wea. Rev.*, **137**, 1250–1271, doi:[10.1175/2008MWR2597.1](https://doi.org/10.1175/2008MWR2597.1).
- , —, L. M. Leslie, M. B. Richman, and C. A. Doswell, 2010: Evaluation of WRF model simulations of tornadic and nontornadic outbreaks that occur in the spring and fall. *Mon. Wea. Rev.*, **138**, 4098–4119, doi:[10.1175/2010MWR3269.1](https://doi.org/10.1175/2010MWR3269.1).

- Thompson, D. B., and P. E. Roundy, 2013: The relationship between the Madden–Julian oscillation and U.S. violent tornado outbreaks in the spring. *Mon. Wea. Rev.*, **141**, 2087–2095, doi:[10.1175/MWR-D-12-00173.1](https://doi.org/10.1175/MWR-D-12-00173.1).
- Trapp, R. J., D. M. Wheatley, N. T. Atkins, R. W. Przybylinski, and R. Wolf, 2006: Buyer beware: Some words of caution on the use of severe wind reports in postevent assessment and research. *Wea. Forecasting*, **21**, 408–415, doi:[10.1175/WAF925.1](https://doi.org/10.1175/WAF925.1).
- Ventrice, M. J., M. C. Wheeler, H. H. Hendon, C. J. Schreck, C. D. Thorncroft, and G. N. Kiladis, 2013: A modified multivariate Madden–Julian oscillation index using velocity potential. *Mon. Wea. Rev.*, **141**, 4197–4210, doi:[10.1175/MWR-D-12-00327.1](https://doi.org/10.1175/MWR-D-12-00327.1).
- Weisman, M. L., and J. B. Klemp, 1984: The structure and classification of numerically simulated convective storms in directionally varying wind shears. *Mon. Wea. Rev.*, **112**, 2479–2498, doi:[10.1175/1520-0493\(1984\)112<2479:TSACON>2.0.CO;2](https://doi.org/10.1175/1520-0493(1984)112<2479:TSACON>2.0.CO;2).
- Wheeler, M., and H. Hendon, 2004: An all-season Real-Time Multivariate MJO index: Development of an index for monitoring and prediction. *Mon. Wea. Rev.*, **132**, 1917–1932, doi:[10.1175/1520-0493\(2004\)132<1917:AARMMI>2.0.CO;2](https://doi.org/10.1175/1520-0493(2004)132<1917:AARMMI>2.0.CO;2).
- Witt, A., M. D. Eilts, G. J. Stumpf, J. T. Johnson, E. D. Mitchell, and K. W. Thomas, 1998: An enhanced hail detection algorithm for the WSR-88D. *Wea. Forecasting*, **13**, 286–303, doi:[10.1175/1520-0434\(1998\)013<0286:AEHDAF>2.0.CO;2](https://doi.org/10.1175/1520-0434(1998)013<0286:AEHDAF>2.0.CO;2).
- Zhang, C., 2005: Madden–Julian oscillation. *Rev. Geophys.*, **43**, RG2003, doi:[10.1029/2004RG000158](https://doi.org/10.1029/2004RG000158).